JET-P(95)63

Feasibility of Quantitative Spectroscopy on ITER

M G von Hellermann, W G F Core, A Howmann, C Jupén[1], R W T König, M F Stamp, H P Summers[2], P R Thomas, K-D Zastrow.

JET Joint Undertaking, Abingdon, Oxfordshire, OX14 3EA, UK.

[1] University of Lund, Sweden.

[2] University of Strathclyde, Scotland.

November 1995

ABSTRACT

The options and needs for a comprehensive spectroscopic diagnostic package on ITER are discussed. Recent JET results illustrate the role of key parameters leading to acceptable levels of data consistency. A high level of accuracy in bulk plasma data, magnetic surfaces and the inclusion of an active beam diagnostic appears to be indispensable for a prospective quantitative spectroscopy on ITER.

INTRODUCTION

Powerful spectroscopic techniques have been developed during the last five decades of fusion research and the understanding of atomic processes in plasmas close to thermo-nuclear conditions has considerably advanced. The main progress has been achieved by the concerted use of several complementary plasma diagnostic systems and the development of appropriate evaluation procedures. The need for consistency checks involving the entire plasma environment has been recognised to play a major role. This is very demanding in terms of data range, quality and integration. In particular, the plasma edge and divertor region is still difficult to assess, so that local or semi-local spectroscopic measurements leading to absolute particle densities rather than incompletely analysed photon counts, are a major challenge.

A crucial part of any quantitative spectral analysis is the deduction of a *local ion velocity distribution function* from a measured spectrum. The experience gained at present fusion devices has clearly demonstrated that *temperature* and *density* are inseparable quantities, and intensity-only or Doppler-width-only measurements can not survive thorough consistency checks. In order to deduce local impurity densities from measured absolute

spectral intensities the *background plasma density* (consisting of electrons, ions and neutrals) and their respective *temperatures* needs to be unambiguously established. In the case of active charge exchange spectroscopy[1,2] the local neutral beam strength is required for the deduction of impurity densities. A precise reconstruction of *magnetic surfaces* enabling the mapping of all plasma data on common flux co-ordinates is an essential part of this procedure.

SPECTROSCOPIC DATA NEEDS

Two examples, the deduction of the *kinetic plasma energy content* and the prediction of *thermal-thermal and beam-thermal neutron rates* are used to highlight key input data necessary for an overall consistency check. The following table summarises the required data and the interdependence of measured and calculated quantities.

Table 1 Reconstruction of kinetic plasma energy and neutron yield from key experimental data. ♦ indicates direct dependence and O weak or indirect dependence. Cross-reference to magnetic field B indicates the need of mapping of data to a common flux grid. B is the result of an equilibrium calculation.

	B	n_e	T_e	T_i	Ω	n_z	$n_{d,th}$	P_{NB}	E_{NB}	v_{crit}	τ_s	ζ	S	$n_{d,fast}$
B		O	O	O	O	O	O							
n_e	♦													
T_e	♦													
T_i	♦				O	O								
Ω	♦			O		O								
n_z	♦	♦	O	O	♦	O		♦	♦			♦		
$n_{d,th}$	♦	♦	O	O	O	♦		O	O	O	O	O	O	♦
W_{th}	♦	♦	♦	♦	♦	♦	♦	O	O	O	O	O	O	O
v_{crit}	♦	♦	♦	O	O	♦	♦	O	O			O		
τ_s	♦	♦	♦											
ζ	♦	♦	O	O	O	♦			♦			O		
S	♦	O	O	O	O	O		♦	♦			♦		
W_{fast}	♦	O	O	O	O	O	O	O	♦	♦	♦	O	♦	
$n_{d,fas}$	♦	O	O	O	O	O	O	O	♦	♦	♦	O	♦	
Y_{dd}^{th-th}	♦	O	O	♦	O	O	♦	O	O	O	O	O	O	O
Y_{dd}^{b-th}	♦	O	O	♦	O	O	♦	O	♦	O	♦	O	♦	

For an ITER plasma with $<Z_{eff}>=1.5$ deuteron densities can be deduced from simultaneous CX measurements of the dominant low-Z impurities (carbon and helium) and electron density data. The dilution is: $d = \frac{n_d}{n_e} = 1 - \sum_{j>1} Z_j \frac{n_j}{n_e}$ (1) and its error: $\frac{\delta d}{d} = \frac{1-d}{d} < \frac{\delta c}{c} >$ (2).
For dilution factors d close to 1 and estimated absolute uncertainties in local impurity concentrations $c_z = \frac{n_z}{n_e}$ of 30% the actual error in dilution values is quite low. For d>0.5 the deduction of deuteron densities from charge neutrality and CX measurements of the main impurities is to be preferred to a direct measurement of deuteron densities[3]. The errors are based on the assumption that electron density profiles can be established reliably by a combination of Thomson scattering (LIDAR) providing precise radial shapes and far infra-

red interferometry providing absolute fringe shifts and thus line integrated electron densities with an accuracy of less than 10%.

Kinetic plasma energy

The thermal ion energy density and the volume integrated kinetic energy content is determined by a CX measurement of radially resolved ion temperature profiles and the main light impurities respectively and the electron pressure measured by Thomson Scattering.

$$W_{thermal} = \frac{3}{2}\int (p_{ion} + p_{electron})dV \quad \text{with } p_{ion}(\rho = r/a) = n_{ion}(\rho)\cdot T_{ion}(\rho) \tag{3}$$

$$\frac{n_{ion,thermal}}{n_e} = (1 - \sum_{z>1} Z\frac{n_z}{n_e}) - \frac{n_{d,fast}}{n_e} + \sum_{z>1}\frac{n_z}{n_e} \tag{4}; \qquad n_d = n_{fast} + n_{thermal} \tag{5}$$

The fast deuteron density is determined by the source rate S of neutral beam injection. For JET two injector boxes with eight neutral beams each contribute to the source rate:

$$S_{tot}(\rho) = \sum_{p=1}^{8}\sum_{k=1}^{3}\frac{f_{k,p}\cdot P_{k,p}}{e\cdot E_{k,p}}\frac{d\zeta_{p,k}(\rho)}{dV(\rho)} \tag{6}$$

$f_{k,p}$: power fraction, $P_{k,p}$: beam power, $E_{k,p}$: neutral beam energy. Indices k and p refer to energy fractions and beam number, ρ=r/a is the minor radius. The neutral beam attenuation factor ζdepends on atomic stopping cross-sections and electron and ion densities:

$$\zeta(\rho) = \exp\left\{-\int ds(\rho)\cdot n_e(\rho)\sum_j \sigma_{stop,j}c_j(\rho)\right\} \tag{7}$$

The effective collision energy between neutral beam and rotating plasma target, which applies for all of the beam energy related calculations, e.g. stopping cross-section, fast particle energy and beam induced neutron rates, is determined by the toroidal plasma rotation and the local pitch angle ($\cos\theta = \frac{R_{imp}}{R}$). For example, in JET hot-ion mode plasmas the rotation induced energy correction may reach values up to 35keV (of 140 keV).

$$E_{col}(\rho) = \frac{1}{2}m_b(\vec{v}_b - \vec{v}_{rot})^2 = \frac{1}{2}m_b(v_b^2 - 2\cdot v_b\cdot R_{impact}\cdot\Omega(\rho) + R^2(\rho)\cdot\Omega^2(\rho)) \tag{8}$$

The fast deuteron density is:

$$n_{fast}(\rho) = \frac{1}{3}\tau_s(\rho)\sum_{p=1}^{8}\sum_{k=1}^{3}S_{k,p}(\rho)\ln[1 + (\frac{v_{col,k,p}(\rho)}{v_c(\rho)})^3] \tag{9}$$

with the slowing-down time:

$$\tau_s(\rho) = \frac{3\pi^{3/2}\varepsilon_0^2}{e^4\ln\Lambda}\frac{m_e m_b}{n_e(\rho)Z_b^2}\left(\frac{2T_e(\rho)}{m_e}\right)^{3/2} \tag{10}$$

and critical velocity:

$$v_c^3(\rho) = \frac{3}{4}\sqrt{\pi}\left(\frac{2T_e(\rho)}{m_e}\right)^{3/2}\sum_j\frac{n_j(\rho)}{n_e(\rho)}Z_j^2\frac{m_e}{m_j} \tag{11}$$

The total fast energy content is calculated from volume integration of the fast particle pressure profile:

$$p_{fast}(\rho) = \frac{1}{2}\tau_s(\rho)\cdot\sum_{p=1}^{8}\sum_{k=1}^{3}S_{k,p}(\rho)E_{col,k,p}(\rho)\left[1 - \frac{2}{3}(\frac{v_c(\rho)}{v_{col,k,p}(\rho)})^2\left\{\begin{array}{l}\frac{1}{2}\ln\frac{v_{col,k,p}^2(\rho) - v_{col,k,p}(\rho)v_c(\rho) + v_c^2(\rho)}{v_{col,k,p}^2(\rho) + 2\cdot v_{col,k,p}(\rho)v_c(\rho) + v_c^2(\rho)} \\ +\sqrt{3}\tan^{-1}(\frac{\sqrt{3}v_{col,p,k}(\rho)}{2v_c(\rho) - v_{col,p,k}(\rho)})\end{array}\right\}\right] \tag{12}$$

Observed and predicted neutron rates

In a beam-heated JET plasma the observed neutron rates are the sum of: Thermal-thermal, beam-thermal and beam-beam neutron rates. The thermal-thermal can be derived from CX ion temperatures and thermal deuteron density profiles:

$$Y_{th-th}(\rho) = \frac{1}{2} n^2_{thermal} < \sigma v_{dd}(T_i(\rho)) > \tag{13}$$

The thermal-thermal d-d reaction rates are calculated using a modified Padé expansion as described in [4]. The beam-thermal neutron rate depends on neutral beam energies, impurity and electron density profiles as well as thermal target density, ion temperatures, toroidal angular rotation frequency Ω. The beam-thermal neutron reactivity and its emissivity profile is:

$$< \sigma v >_{b-th} = \int_0^{v_{b,p,k}} \frac{v^2 dv}{v^3 + v_c^3(\rho)} \cdot \frac{2}{m \cdot v} \cdot P(\frac{1}{2} m v_{th}^2 u_l^2) \sqrt{\frac{u_l^3}{u_l^3 + \alpha}} \cdot \exp\left\{ -\left[(u_l - \frac{v}{v_{th}})^2 + \frac{\alpha}{u_l} \right] \right\} \tag{14}$$

$$Y_{b-th}(\rho) = n_{thermal}(\rho) \cdot \tau_s(\rho) \cdot \sum_{p=1}^{8} \sum_{k=1}^{3} S_{p,k}(\rho) \cdot < \sigma v >_{b-th} (\rho, p, k) \tag{15}$$

with $\alpha = \sqrt{\frac{2B^2}{m v_{th}^2}}$ and $2u_l^2(u_l - \frac{v}{v_{th}}) - \alpha = 0$

P is the Padé function and B a constant.

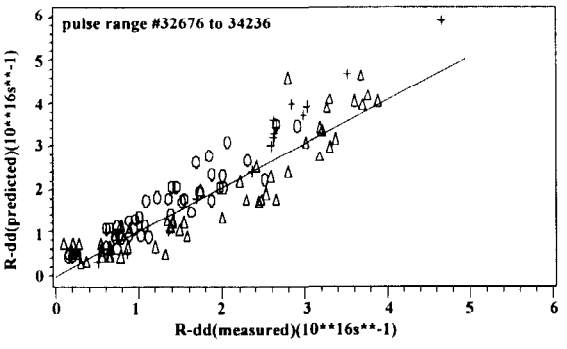

Fig.1 Comparison of predicted (see table I and equations above) and measured neutron yield

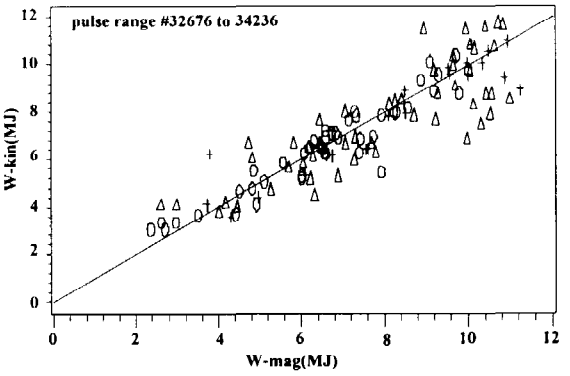

Fig.2 Comparison of kinetic (eqn.(3)) and diamagnetic energy content

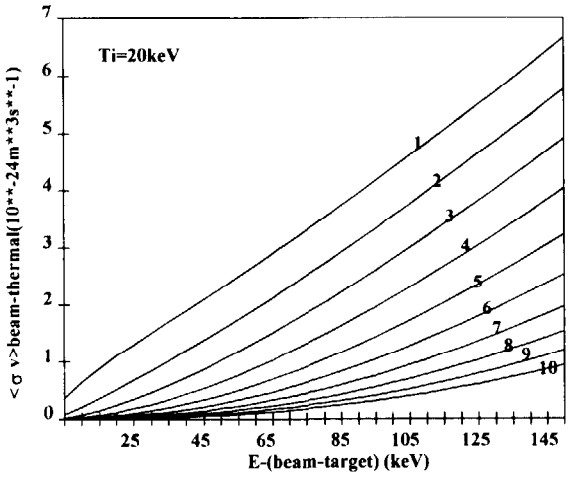

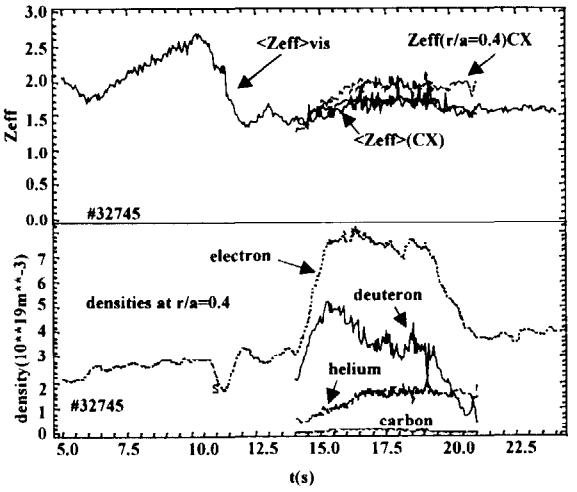

Fig. 3 Beam-thermal averaged reaction rate (eqn.13). Numbers 1 to 10 refer to critical velocity in steps of $5 \cdot 10^5$m/s.

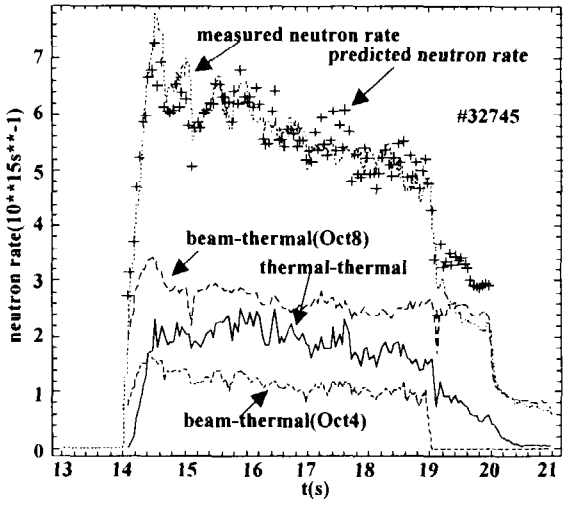

Fig. 5 Measured and predicted (eqns.(12, 13, 14)) thermal-thermal and beam thermal neutron rate in a radiative divertor plasma

Fig.4 a) <Zeff> from bremsstrahlung and profile averaged CX data in a radiative divertor plasma b) impurity and bulk plasma densities

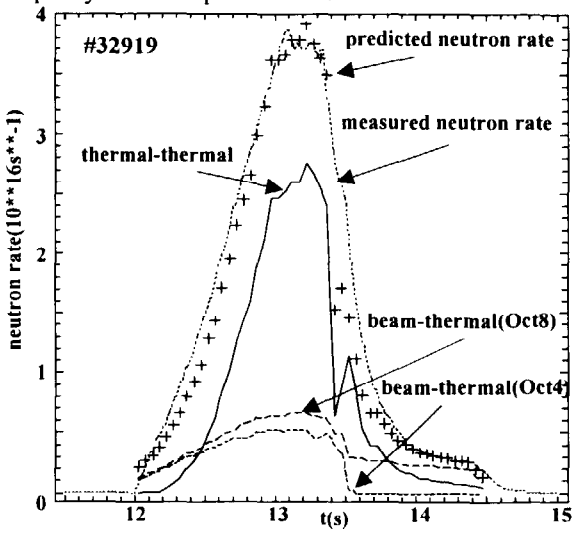

Fig. 6 Measured and thermal-thermal and beam thermal neutron rate in a hot-ion mode plasma

FEASIBILITY OF AN ACTIVE BEAM DIAGNOSTIC ON ITER

The chapter addresses three specific problems related to the feasibility of an active beam diagnostic on ITER. One is the role of *background spectral lines* emitted at the plasma edge, the second is the *detection of weak CX spectra* with amplitudes comparable to fluctuations of the continuum background radiation, and finally, what must be considered a fundamental bottle-neck, the *error propagation of the neutral beam attenuation* calculation.

Background spectral emission

This is the most difficult part to assess in advance of an ITER operation. Experience at JET and other tokamaks have shown that viewing lines looking onto wall sections close to high recycling areas may lead to complex passive emission spectra with appreciable signal levels. As a rule of thumb, if neighbouring edge line intensities exceed that of the active CX signal by more than order of magnitude any quantitative analysis (that is unambiguous extraction of a velocity distribution function) is put at risk. This applies in particular to the analysis of the CX HeII spectrum where intense CIII, CIV and BeII lines affect the analysis. The high quantum shell edge lines of CIII, CIV and BeIV are currently investigated [5]. Only sparse data exist on edge emissions close to CX spectra in the UV wavelength region [6] but present results indicate an even greater complexity of passive background line emissions. A UV CX spectroscopy for ITER appears therefore not to be a true alternative.

Signal-to-Noise considerations

In the case where fluctuations of the continuum radiation signal is the dominant noise source in an observed charge exchange spectrum, and passive line emission is not significant, the signal-to- noise can be expressed by, cf. [7] :

$$\{\frac{S_z}{N}\} = \frac{I_n c_z \sigma_{CX} \exp\{-\int dr n_e \sum_z c_z \sigma_{s,z}\}}{\pi w_\perp e \sqrt{Z_{eff} G_{ff} L_p B_c}} \sqrt{\frac{c \cdot v_e}{v_z^2}} \sqrt{\Delta t \frac{\Delta\lambda}{\lambda} \Re} \qquad (16)$$

I_n : neutral beam current, $I_{neutral} = e \cdot n_{beam} \cdot v_{beam} \cdot A_{beam}$

A_{beam} : beam area, $A_{beam} = \pi \cdot w_\perp \cdot w_{l.o.s}$

n_z , $c_z = n_z/n_e$: impurity ion density and its relative concentration

Δt : integration time

$\Delta\lambda$: spectral wavelength interval

$\Re$: detection efficiency ($\Re = t \cdot \eta \cdot \varepsilon$ is the number of counts per radiance, with t : optical transmission, η : detector quantum efficiency, ε : spectrometer étendue $\varepsilon = \Delta\Omega \cdot A_{sp}$

σ_{cx} : CX emission cross section.

σ_{sz} : effective neutral beam attenuation stopping rate, including electron and ion impact ionisation as well as charge exchange processes

G_{ff} : free-free Gaunt factor

L_p : effective length of the continuum line-of-sight integration:

$$\frac{< n_e^2(0) > L_p}{T_e^{1/2}(0)} = \int ds(r) \frac{n_e^2(r)}{T_e^{1/2}(r)},$$

$$B_c = \left[\frac{e^2}{4\pi\varepsilon_0}\right]^3 \frac{16}{3hc^4 m_e^2} \sqrt{\frac{\pi}{3}}$$

Z_{eff} :effective plasma ion charge:

$$Z_{eff} = 1 + \sum_{z>1} c_z \cdot Z_z \cdot (Z_z - 1) \qquad (17)$$

Fundamental limits for a quantitative CX diagnostic

A crucial part in the deduction of a local impurity densities from measured CX photon fluxes is the ability to provide accurate local neutral beam density data. The local beam strength is determined by stopping cross-sections (Fig.7) as well as electron, impurity densities and temperature profiles. The error in the deduced density introduced by an error in the attenuation is given by:

$$n_z = \frac{4\pi\phi_{cx}}{n_b L_{cx} \langle\sigma v\rangle_{cx}}$$

$$n_b = n_b(0) e^{-\int dr n_e \sum_z \sigma_{sz} c_z}$$

$$\frac{\Delta n_z}{n_z} = \frac{\Delta n_b}{n_b} \approx \frac{\Delta(\sigma_{sz}, n_e)}{(\sigma_{sz}, n_e)} \cdot \sum_z \sigma_{sz} c_z \cdot \int_{plasma-boundary}^{cx-volume} ds \cdot n_e \qquad (18)$$

A convenient approximation for the relative error at 100 keV/amu (neglecting in a first approximation the contributions of impurities) is given by:

$$\frac{\Delta n_z}{n_z} \approx \frac{\Delta n_b}{n_b} \approx 2 \cdot \frac{\Delta x}{x} < n_e L / 10^{20} m^{-2} >_{cx-pl.bdy.} \qquad (19)$$

For example, a relative error $\frac{\Delta x}{x} = 0.1$ of the main input data (primarily the electron density) implies that, due to the exponential decay of the beam strength along the penetration path into

the plasma, at an attenuation factor of $\zeta<0.05$ the errors in beam strength exceed 50%. A further option, cf. [3], which is currently explored, is the use of active Balmer Alpha beam emission spectroscopy for an independent experimental deduction of local neutral beam strength. This alternative technique, which is still in its infancy, will become attractive once its experimental errors are proven to be less than the exponential errors introduced by the beam attenuation calculation.

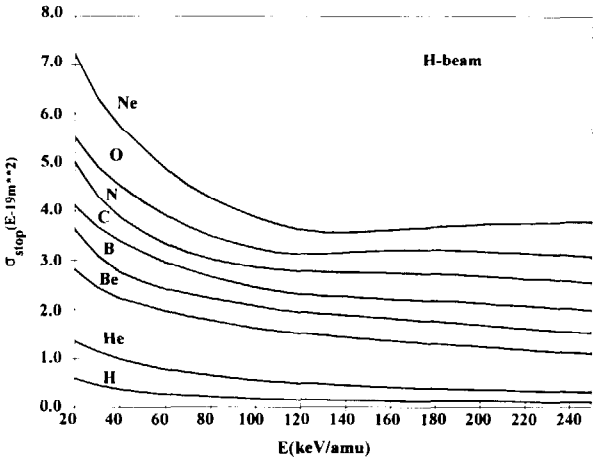

Fig.7 Total stopping cross-sections for a hydrogenic neutral beam (H^0, D^0) interacting with the main light impurities in a plasma. The total cross-section refers to the sum of electron and ion ionisation and charge exchange interactions.

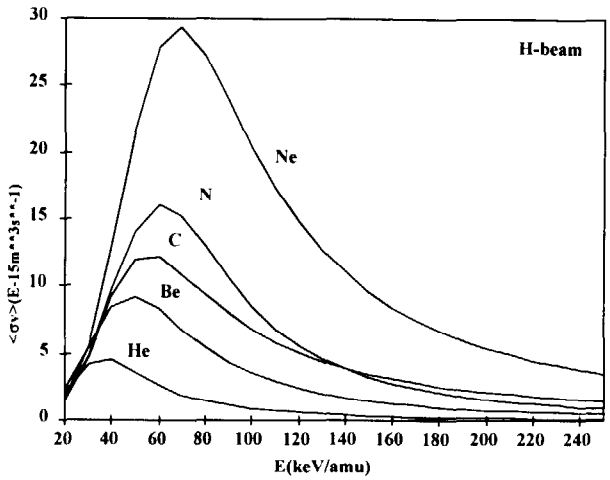

Fig.8 Effective emission rates for CX transitions He(n=4→3, 4685.25Å), Be(n=6→5, 4658.55Å), C(n=8→7, 5290.5Å), N(n=9→8, 5671Å) and Ne(n=11→10, 5249.7Å) for a hydrogenic neutral beam (D^0 or H^0) as an electron donor.

DIAGNOSTIC BEAM OPTIMISATION

The signal-to-noise (equation (16)) depends approximately linearly on the impurity concentration c_z since its occurrence in Z_{eff} leads only to a weak modification ($1<Z_{eff}<2$). For an optimised operation of a fusion reactor the helium ash level is constant and needs to be kept below approximately 10% of the electron density. The signal-to-noise ratio is therefore primarily determined by the energy dependencies for CX excitation rates and beam stopping cross-sections respectively. Most of the CX excitation rates for low-Z impurities (cf. Fig.8) reach a maximum at about 50 keV/amu (HeII(4→3)@37keV/amu, CVI(8→7)@49keV/amu and NeX(11→10)@63keV/amu) whereas beam-stopping cross-sections continuously decay with increasing beam energy. If there were no limits to power supplies, neutral beam designs etc. one could consider an apparent gain by pushing the beam energies to higher levels. However the excitation rates for charge exchange recombination radiation drop more rapidly than the gain in beam penetration (Fig.7 and Fig.8).

The following beam optimisation study is dictated by technical constraints given by the ITER environment. Neutral beam ion sources must be shielded from magnetic stray fields. This implies a location of the source at a considerable distance away from the toroidal field coils. At the same time a high neutral current density (minimisation of $w_\perp$) must be maintained in the plasma centre for an optimisation of the signal to noise ratio. This leads to the requirement of a low-divergence neutral beam. Present day neutral beam technologies based on the development of negative ion sources promise a gain in beam divergence compared to positive ion sources. High power negative ion beam sources, which are presently under construction cf. [9] have specifications coming close to data estimated for spectroscopic optimisation studies as presented in this paper.

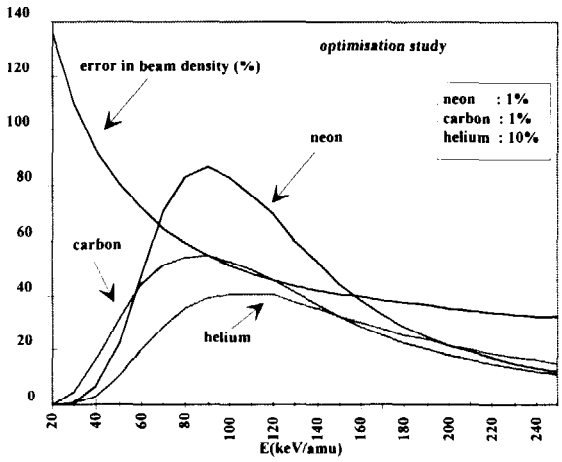

Fig.9 Figure of merit (a.u.). for the detection of CX spectra of helium (10%), carbon (1%) or neon (1%). The ITER central target density is $10^{20}m^{-3}$. The error in beam density is calculated for that impurity composition and target density. The beam neutral current is assumed to be constant over the energy range.

Table II Comparison of JET CX spectroscopy related diagnostic beam data and extrapolation to ITER

	JET	ITER
ion type	positive ion source	negative ion source
effective beam power for CX diagnostic (MW)	2	10
beam species	T^0,D^0	H^0
energy (keV/amu)	53 or 65	120
neutral beam current (full energy)	30 A	80 A
beam divergence	0.8°	0.2°
distance ion source plasma centre (m)	11.0	30
beam dimensions in plasma centre (m)	$w_{\perp}$=0.15, $w_{l.o.s.}$=0.15	$w_{\perp}$=0.1, $w_{l.o.s.}$=0.3
central target density (m^{-3})	$5 \cdot 10^{19}$	$10 \cdot 10^{19}$
beam path length (m)	1.2	2.8
line integral to centre (m^{-2})	$6 \cdot 10^{19}$	$20 \cdot 10^{19}$
impurity composition	D(74%),He(10%),C(1%)	D(74%),He(10%),C(1%)
emission rates ($10^{15}m^3s^{-1}$)	3.6 12.2	0.56 5.09
Z_{eff}	1.26	1.26
beam attenuation	0.12	0.013
error in beam attenuation	21%	43%
integration time	0.05s	0.5s
detection sensitivity $\frac{\text{counts/s}}{(\text{photons/s/sr/cm}^2)}$	10^{-6}	$5 \cdot 10^{-6}$
path length for continuum radiation (m)	6	12
figure of merit (CVI spectrum)	55	43

COMPLEMENTARY ION TEMPERATURE DIAGNOSTICS

Any passive ion temperature diagnostic, e.g. X-ray emission spectroscopy, neutral particle energy analysis or neutron spectroscopy represents a line-of-sight integrated, and therefore *non-localised* measurement. This necessitates local values to be reconstructed either by tomographic techniques, which requires a substantial number of viewing lines, or the calculation of location and radial width of emission shells. Recent results at JET, cf. [8], have

demonstrated that by choosing an off-axis X-ray line-of-sight for the collection of NiXXVII spectra, a comparatively narrow emission shell contributing to the signal may arise and consequently a reduced uncertainty in the radial position is gained. The method is based on the local emissivity, which is calculated from electron density and electron temperature profile data, providing thus a weighting function which leads to an *expectation value* and its *variance* of the magnetic flux surface at which the line of sight integrated X-ray spectrum is dominantly emitted.

$$<\rho>=\frac{\int \rho \cdot w(\rho) d\rho}{\int w(\rho) d\rho} \quad \text{with}: w(\rho) = f_{NiXXVII}(T_e(\rho)) \cdot n_e^2(\rho) \cdot \varepsilon(T_e(\rho)) \cdot g(\rho) \qquad (20)$$

f is the local fraction of helium-like nickel, ε the emissivity, and g a geometry factor. The width of the emission layer:

$$\sigma_\rho = \sqrt{<\rho^2> - <\rho>^2} \qquad (21)$$

is calculated by the second moment of the same weighting function. For the present geometry of the JET divertor phase typical variances are $\sigma_\rho = \pm 0.2$ that is radial uncertainties are 20% of the minor radius. In theory it would be a possible option for ITER to design a passive ion temperature diagnostic system consisting of a fan of x-ray lines-of-sight each dedicated to a specific ion stage and to reconstruct a finite number of ion temperature values and their respective emission shell positions.

ALTERNATIVE LOW-Z ION DENSITY DIAGNOSTICS ?

There is to the present knowledge no alternative to active beam based charge exchange spectroscopy which may provide *local density data* of low-Z impurities (fully stripped helium, carbon, beryllium, boron etc.) with sufficient accuracy. If, for example, helium ash densities are to be deduced from (visible) continuum radiation measurements and of line averaged Z_{eff} values, this would have to rely on a known impurity composition (e.g. 1% C, 1%Be). For a 10% level of helium changes in Z_{eff} of the order 0.2 have to be measured:

$$<Z_{eff}> = 1 + \sum Z(Z-1)\frac{n_z}{n_e} \text{ or } <\frac{n_{He^{2+}}}{n_e}> = \frac{<Z_{eff}>-1}{2} - 15 <\frac{n_{C^{6+}}}{n_e}> \qquad (22)$$

This implies that $<Z_{eff}>$ values have to be measured with an absolute accuracy of better than 0.05 which puts unrealistic demands on the accuracy of radial electron density and temperature profiles. Moreover, this is already the optimum accuracy of the absolute calibration of the measured bremsstrahlung.

The deduction of radial helium profiles from multi-chord bremsstrahlung measurements is even more doubtful. Uncertainties in Abel inversion procedures, in particular for the case for flat or hollow impurity profiles, exceed by far required data accuracies. Similar arguments apply for the use of tomographic reconstruction of x-ray emission profiles where accurate electron density and temperature data and impurity compositions will be needed for the deduction of a single low-Z impurity.

ABSOLUTE AND CROSS-CALIBRATION OF SPECTROSCOPIC INSTRUMENTS

There is one important aspect related to the measurement of line integrated continuum radiation and the deduction of $<Z_{eff}>$ which plays a central role for the deduction of absolute densities. This is the provision of an established cross-calibration source in addition to primary absolute calibrations. In most of the present fusion experiments, and this applies even more for ITER, in situ absolute calibrations during extended periods of operation are

difficult, if not entirely impossible. Provided Z_{eff} is a constant on a magnetic flux surface and each spectroscopic line of sight can be characterised by its impact minor radius ρ_{imp} then cross-calibrations of spectroscopic instruments with arbitrary lines of sight can be established at any time.

$$< Z_{eff}(\rho_{imp}) >= \frac{\int_{\rho_{imp}}^{1} I_{cont}(\rho)\frac{ds}{d\rho}d\rho}{B_c \int_{\rho_{imp}}^{1} d\rho \frac{ds}{d\rho}\frac{n_e^2(\rho)\cdot g_{ff}(1,\rho)}{\lambda\cdot\sqrt{T_e(\rho)}}} \qquad (23)$$

The constant B_c is defined in eqn. (16) and the integration ds refers to the path along the line-of-sight and dρ its corresponding increment in magnetic flux co-ordinate or normalised minor radius.

SUMMARY

The experiences at the JET experiment and also other major fusion devices have shown that the measurement of high accuracy ion temperature profiles is central for the control and analysis of plasmas close to thermo-nuclear conditions. Active beam techniques provide to the present knowledge the only access to profiles with the required accuracy ($\frac{\Delta T}{T} < 0.1$ and $\frac{\Delta r}{r} < 0.05$). A prerequisite for a quantitative CX deduction of impurity and deuteron densities is the availability of accurate data on electron density and temperature and also the provision of magnetic data. The deduction of local ion densities with errors less than 30% should be feasible. Adequate neutral beam sources with sufficient energy, power etc. for an active beam diagnostic on ITER do exist and should not be a problem. However, fundamental limits for a CX diagnostic dictated by errors in calculated beam attenuation factors, corresponding to an upper line density along the beam path of $2\cdot10^{20}$ m^{-2}, emphasise the need for additional passive techniques, for example, X-ray spectroscopy or neutron spectroscopy providing complementary, less-localised ion temperatures values. There is no alternative for thermal alpha particle or, in general, for low-Z impurity concentration measurements except by CX spectroscopy.

REFERENCES

1. R.Isler, Plasma Physics and Contr. Fusion, **36**, 171(1994)
2. M. von Hellermann and H.P.Summers, Atomic and Plasma Material Interaction Processes in Controlled Thermonuclear Fusion, Ed. Janev, 'Elsevier Science Publishers 1993',135-164
3. W.Mandl, R.Wolf, M von Hellermann, Plasma Phys. Contr. Fusion,**35**,1373, 1993
4. H.S.Bosch, G.M. Hale, Nuclear Fusion **32**,611(1992)
5. C.Jupen, I. Martinson, M. Tunklev, University of Lund, Sweden, to be published
6. H.W.Morsi, R.W.T. König, H. Schröpf, M.G. von Hellermann
   Accepted for publication in Plasma Physics and Controlled Fusion, JET-P(95)24
7. M von Hellermann, W.G.F.Core, J.Frieling, L.D.Horton, R.W.T. König, W.Mandl, H.P.Summers, Plasma Phys. Contr. Fusion,**35**,799, 1993
8. M. von Hellermann, P. Breger, W.G. Core, U. Gerstel, N.C.Hawkes, A. Howman, R.W.T. König, C.F. Maggi, A.C. Maas, A.G. Meigs, P.D. Morgan, J. Svensson, M.F. Stamp, H.P. Summers, R.C. Wolf, K.-D. Zastrow, Proc. ICPP 1994, Foz do Iguacu, Brazil, Nov. 94, JET-P(94)58
9. Iiushi et al., Proc. ICPP 1994, Foz do Iguacu, Brazil, Nov. 94